Ongoing habenular activity is driven by forebrain networks and modulated by olfactory stimuli

Ewelina Magdalena Bartoszek[1], Suresh Kumar Jetti[2], Khac Thanh Phong Chau[1], Emre Yaksi[1*]
1Kavli Institute for Systems Neuroscience and Centre for Neural Computation, Faculty of Medicine and Health Sciences, Norwegian University of Science and Technology, Olav Kyrres gata 9, 7030 Trondheim, Norway.
2Neuro-Electronics Research Flanders, 3001 Leuven, Belgium.
[*] Corresponding authors: emre.yaksi@ntnu.no

SUMMARY
Ongoing neural activity, which represents internal brain states, is constantly modulated by the sensory information that is generated by the environment. In this study, we show that the habenular circuits act as a major brain hub integrating the structured ongoing activity of the limbic forebrain circuitry and the olfactory information. We demonstrate that ancestral homologs of amygdala and hippocampus in zebrafish forebrain are the major drivers of ongoing habenular activity. We also reveal that odor stimuli can modulate the activity of specific habenular neurons that are driven by this forebrain circuitry. Our results highlight a major role for the olfactory system in regulating the ongoing activity of the habenula and the forebrain, thereby altering brain's internal states.

INTRODUCTION
Continuous interactions between the sensory world and the internal states of the brain are essential for survival. For example, a sudden change in the environment by the presence of a salient sensory cue can be critical for updating an animals' brain from its resting to an alert state [1-3]. Seminal studies in human subjects clearly demonstrated the presence of such rapid alterations from a default state with high levels of brain activity [4, 5] to an alert state with reduced levels of global network activity and increased activity in sensory or attention related areas during various tasks [3, 6, 7]. While the precise definition of a 'brain state' can vary depending on the time scales of investigated phenomena, the link between ongoing (or spontaneous) brain activity and the current state of the brain is well accepted [8-14]. In fact, ongoing neural activity has been observed across the nervous system, from brain areas involved in sensory processing [15-23], to innate behaviors [24-26], and higher cognitive function [27-37]. Despite the presence of ongoing activity across the brain and its rapid alterations coupled with brain state transitions, dedicated neural pathways and their connection to ongoing brain activity and sensory-evoked transitions remain to be identified.
One brain region that receives information from both sensory [38-40] and cortico-limbic [41-54] brain structures, and exhibits high level of ongoing neural activity, is the habenula. This evolutionary conserved diencephalic nucleus [44, 55-57] is a major hub relaying information from diverse forebrain inputs [41, 43-48, 50, 58] to its target regions that directly control animal behavior via the release of dopamine, acetylcholine, and serotonin [40, 44, 45, 59-69]. Previous studies established a direct role for the habenula in adaptive behaviors [8, 64, 65, 70-74], learning [45, 47, 64, 73, 75, 76] and prediction of outcomes [45, 71, 75, 77, 78]. Not surprisingly, habenular dysfunction is closely linked to several neurological conditions and mood disorders including depression [54, 79]. Based on molecular profiles [80-85], anatomical landmarks [64, 73, 76, 86], and neural activity [52, 53, 64, 87], habenula is divided into numerous subdomains. Most prominent in zebrafish are the dorsal (dHb) and the ventral habenula (vHb), which are the homologous to mammalian lateral and medial habenula [64, 73, 76, 86], respectively. dHb is involved in sensory processing [40, 67, 88], circadian rhythms [67], social behaviors [72] and experience-dependent fear response [65, 73, 76]. Whereas vHb plays important roles in learning [64] and active coping behavior [8]. Recent studies showed that ongoing neural activity associated with the transition between brain states is present in both dHb and vHb [8, 52, 53, 65]. Interestingly, sensory cues that have been shown to induce prominent behavioral responses in zebrafish [8, 65, 66, 83, 89-91], were also shown to elicit distinct neural responses both in dHb [39, 52, 65, 87] and vHb [8, 52]. Yet, it is less clear how ongoing habenular activity is generated by the distributed brain networks and how this ongoing activity interacts with sensory responses in the habenula and across the brain.
In this study, we investigated how interactions between ongoing and sensory-evoked activity can shape brain's internal states, in the habenula and across the entire zebrafish forebrain. First, we showed that functional interactions of neurons within distinct habenular subdomains are stable and spatially organized across different periods of ongoing activity. Next, we revealed that ongoing habenular activity is driven by the ancestral homologs of limbic forebrain regions, hippocampus and amygdala. Finally, we demonstrated that olfactory cues switch the internal states of the habenula by specifically modulating the activity of habenular neurons driven by ancestral limbic forebrain regions. Our results reveal that the habenula acts as a hub integrating limbic and sensory signals, and olfactory cues switch internal brain states by inhibiting the ongoing activity of the habenula and its ancestral limbic forebrain inputs.

RESULTS
Structured ongoing activity in the habenula is stable over time

To investigate ongoing habenular activity, we performed volumetric two-photon calcium imaging across the entire habenula of juvenile Tg(elavl3:GCaMP6s) zebrafish [52, 92-94], expressing GCaMP6s panneuronally. In all our experiments, we used 3 to 4-weeks-old zebrafish that were shown to exhibit complex behaviors such as learning [75, 95, 96] and social interactions [97, 98], which are mediated by habenular circuits [64, 72, 73, 75, 78]. We observed structured ongoing activity across the entire habenula (Figure 1A), in line with earlier studies focusing on the dHb [53]. To quantify ongoing habenular activity, we performed k-means clustering on habenular calcium signals and observed that distinct functional clusters of habenular neurons exhibit synchronous activity (Figure 1A, B, Figure S1). Next, we investigated, whether such functional clusters in habenula are stable across different time periods, by comparing the activity of functional clusters that were recorded in two consecutive time windows. We quantified the stability of habenular clusters by measuring the probability of a pair of habenular neurons in the same cluster during period #1 to remain in the same clusters in period #2, which we termed "cluster fidelity" [52, 53]. We observed that more than 40% of habenular neuron pairs remained in the same cluster, which is significantly above chance levels (Figure 1C). The functional clusters of habenular neurons identified by k-means clustering appeared to be spatially organized across the entire habenula (Figure 1B, Figure S1). To quantify the spatial distribution of the synchronous habenular activity, we plot the average pairwise correlation of neurons versus the distance between them. We observed that nearby habenular neurons exhibit more correlated/synchronous ongoing activity, when compared to distant pairs of neurons within each habenular hemisphere (Figure 1D). Our results using k-means clustering of ongoing habenular activity suggest that while neurons within the same clusters exhibit highly correlated activity (i.e. within individual clusters of Figure 1A), neurons in different clusters can also be anti-correlated (i.e. between cluster #3 and cluster#5 of Figure 1A). We investigated whether such correlations and anti-correlations between habenular neurons are stable across different time periods, by plotting pairwise correlations of all recorded neuron pairs. In fact, we observed that correlations and anti-correlations

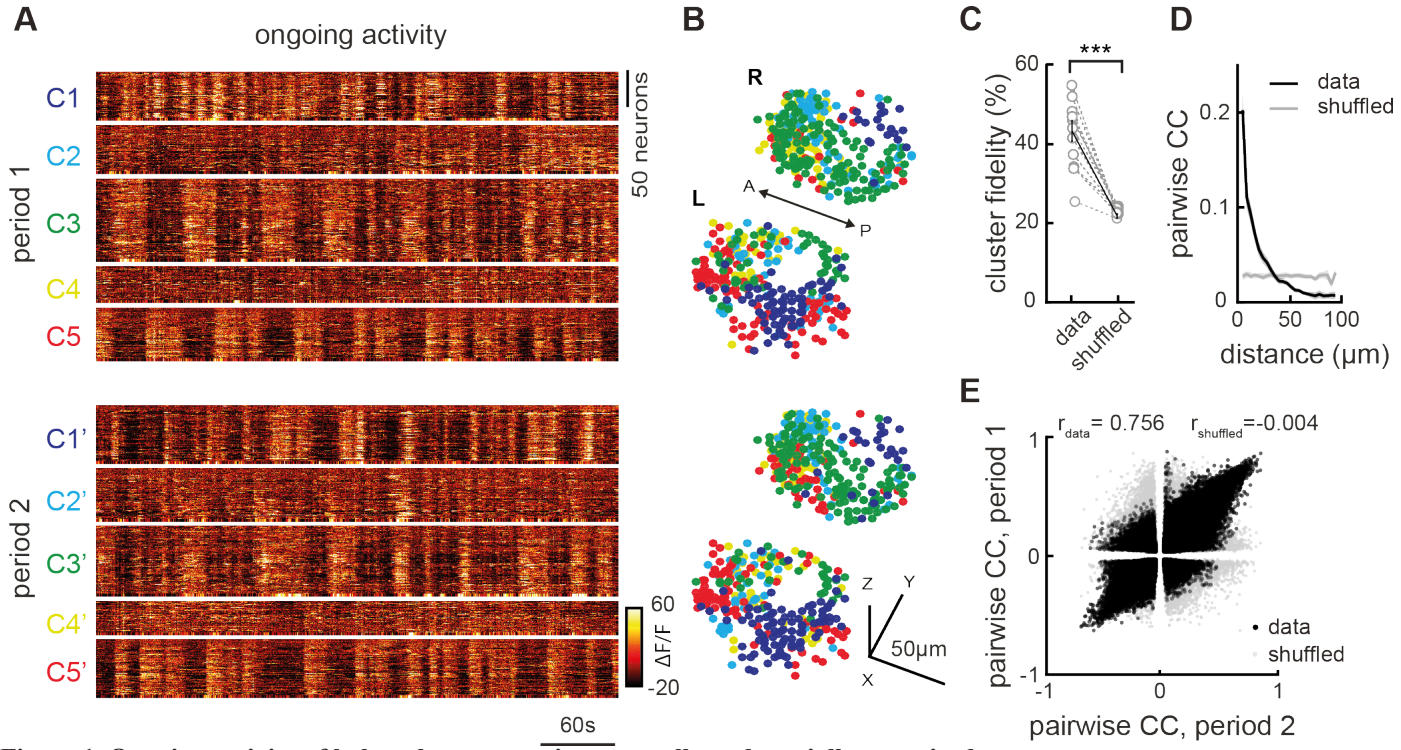

Figure 1. Ongoing activity of habenular neurons is temporally and spatially organized
(A) Representative example of ongoing habenular activity recorded by two-photon calcium imaging in Tg(eval3:GCaMP6s) zebrafish line. Habenular neurons are clustered (C1-5) using k-means clustering over two consecutive time periods of 7 minutes each (period 1 – top and period 2 – bottom). Warm colors represent higher calcium signals. (B) Representative example of three-dimensional reconstruction of habenular neurons clustered using k-means clustering in two consecutive time periods (top, bottom). Neurons are color-coded based on their cluster identity that correspond to the calcium signals depicted in A. L – left; R – right hemisphere, A – anterior, P – posterior. (C) The ratio of habenular neuron pairs remaining in the same functional clusters (high cluster fidelity) is significantly higher than chance levels, during two different time periods of ongoing activity. 315 ± 35 (mean ± SEM) habenular neurons were imaged in each fish (n=11 fish). ***p<0.001, Wilcoxon signed rank test. (D) Relation between pairwise correlation of habenular neurons during ongoing activity and the distance between each neuron pair. Grey line represents shuffled spatial distributions. (E) Pairwise correlations of calcium traces of habenular neurons (with p-value<0.05) during two consecutive time periods, in black. Grey dots represent pairwise comparison that are shuffled for pair identities. Actual data exhibit a correlation of rdata=0.756 for the pairwise correlation across two time periods, indicating robust synchrony between pairs of neurons. Shuffled distribution is rs=-0.004.

between habenular neurons remained stable across different time periods (Figure 1E, black), and this relationship was different from shuffled distributions of such pairwise relationships (Figure 1E, grey). Taken together, these results revealed that the ongoing habenular activity is highly structured, stable over time, and spatially organized into functional clusters of habenular neurons exhibiting synchronous or anti-synchronous ongoing activity.

Distinct forebrain regions correlate with ongoing habenular activity

Previous studies in mammals [45, 47, 48, 50, 99-103] and in zebrafish [39, 41, 52, 53, 65, 67, 72, 73, 75, 80, 87] showed that several forebrain regions send anatomical projections to the habenula. We asked which of these candidate forebrain regions might drive and modulate ongoing habenular activity. To do this, we measured the ongoing activity of the entire forebrain of the juvenile zebrafish, including the habenula, by using volumetric two-photon calcium imaging. To identify forebrain regions that might drive distinct functional clusters of habenula, we asked which forebrain neurons are most correlated with the average ongoing activity of individual habenular clusters (Figure 2A, B). We observed that the neurons of dorsolateral (Dl), dorsomedial (Dm), ventrodorsal forebrain (Vd), and the olfactory bulbs

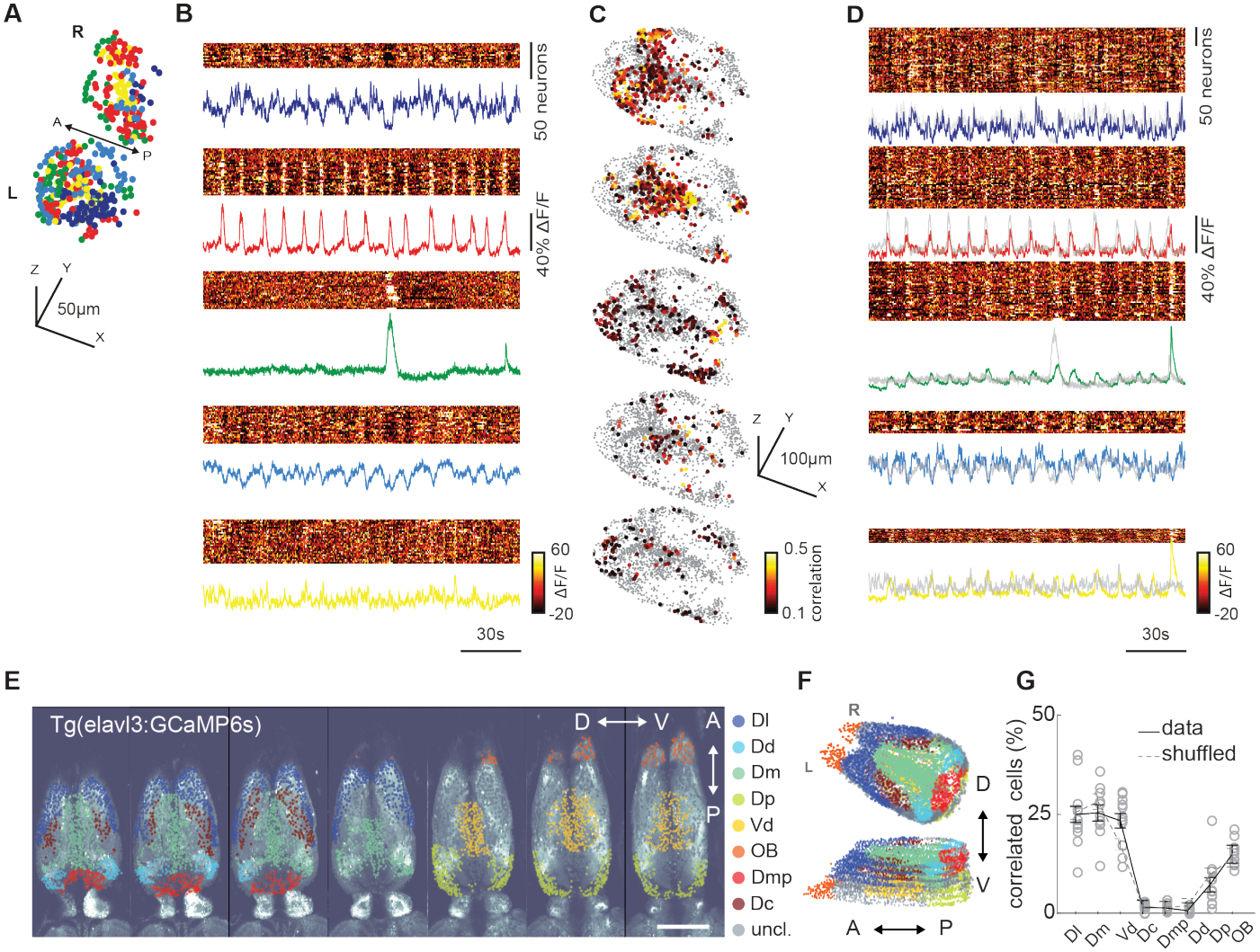

Figure 2: . Ongoing activity of habenular neurons is correlated with sensory and limbic forebrain regions.
(A) Reconstruction of habenular neurons in Tg(elavl3:GCaMP6s) zebrafish, clustered with k-means clustering. Colors represent clusters with similar ongoing activity. L-left; R-right hemisphere. 315 ± 35 (mean ± SEM) habenular neurons were imaged in each fish (n=11). (B) Ongoing activity of the habenular neurons corresponding to clusters in A. Warm colors represent higher activity. Color-coded traces represent the average activity of all neurons in each cluster. (C) Reconstruction of forebrain neurons that are strongly correlated (Pearson's correlation >0.1) to average ongoing activity of habenular clusters in B. Warm colors represent stronger correlations. 2135 ± 345 (mean ± SEM) forebrain neurons were imaged in each fish (n=11 fish). (D) Ongoing activity of the forebrain neurons corresponding to clusters of neurons depicted in C. Color-coded traces represent the average activity of neurons in each cluster. Grey traces represent the average activity of habenular clusters in B. Note that the ongoing activity of identified forebrain neurons and habenular clusters are highly similar. (E) Forebrain regions identified based on anatomical land marks are color coded, and overlaid on raw two-photon microscopy image. Scale bar represents 100um. Optical planes are shown from dorsal to ventral. A – anterior, P – posterior, D – dorsal, V – ventral. (F) Reconstruction of forebrain regions shown in E. (G) Distribution of forebrain neurons with strong correlation (>0.1) to ongoing habenular activity into anatomically identified forebrain regions. Dl – dorsolateral telencephalon, Dd – dorsal nucleus of the dorsal telencephalon, Dm – dorsomedial telencephalon, Dp – posterior zone of the dorsal telencephalon, Vd – dorsal nucleus of the ventral telencephalon, OB – olfactory bulb, Dmp – posterior nucleus of dorsomedial telencephalon, Dc – central zone of the dorsal telencephalon. Black lines represent mean ± SEM.

(OB) contained neurons with highest correlations to individual habenular clusters (Figure 2C, D, Figure S2).

To identify and quantify the forebrain regions driving habenula, we manually delineated distinct forebrain nuclei using anatomical landmarks that were identified by previous studies in zebrafish [38, 104-113] and in other teleosts [114-122] (Figure 2E, F). To further test whether anatomically identified forebrain regions overlapped with functionally distinct forebrain clusters, we compared those manually delineated forebrain nuclei (Figure S3A, B) with k-means functional clusters of ongoing forebrain activity (Figure S3C). We quantified this overlap with a previously used cluster selectivity index [52, 53]. Cluster selectivity would be "0" if all neurons of an anatomically delineated nuclei were randomly distributed to different functional clusters, or "1" if all neurons of the nuclei were in the same functional cluster. In fact, our results showed that cluster selectivity is significantly higher than the chance levels for all forebrain regions (Figure S3D), suggesting that the neurons of manually delineated forebrain regions are selective to one or few functional clusters. Next, we asked in which of these forebrain regions we can find neurons that are strongly correlated (Pearson's correlation above 0.1) with the average ongoing activity of each habenular cluster. Our results revealed that the dorsolateral (Dl), dorsomedial (Dm), and ventrodorsal (Vd) telencephalic regions, homologous to mammalian hippocampus [120, 121, 123-126], amygdala [106, 116, 124, 125, 127, 128] and striatum [55, 124, 129] respectively, contains the largest fraction of habenula correlated neurons, in addition to the olfactory pathway (Figure 2G). These results suggest that ancestral homologs of mammalian limbic forebrain circuits in zebrafish, Dl, Dm, Vd, are potential candidates to drive ongoing habenular activity.

Electrical micro-stimulation of limbic forebrain regions Dl and Dm elicits spatially organized responses in the habenula

Our correlation-based functional connectivity measurements (Figure 2) suggest that distinct limbic forebrain regions might be the major drivers of ongoing habenular activity. To test this hypothesis directly, we locally activated dorsal forebrain by a glass micro-stimulation electrode while measuring forebrain and habenular activity, in a juvenile zebrafish brain-explant preparation with intact connectivity [93]. Inserting the micro-stimulation electrode in Dl or Dm allowed direct activation of these dorsal forebrain regions (Figure 3A, J). Micro-stimulation of Dl and Dm also elicit significant activation in 23-29% of habenular neurons (Figure 3B, C, K, L), that are spatially organized (Figure 3D, M). Application of glutamate receptor blockers (AP5/NBQX) silenced habenular responses (Figure S4), confirming that the habenular responses upon forebrain micro-stimulation is not due to direct electrical activation of habenula, but due to glutamatergic inputs received by the habenular neurons. Due to its intact connectivity, juvenile zebrafish brain-explant exhibits sufficient level of structured ongoing habenular activity to identify functional clusters in habenula by using k-means clustering (Figure 3E, F, N, O). We observed that ~40% of habenular neurons (significantly higher than chance levels) within a given functional cluster remained in the same cluster during forebrain micro-stimulation of Dm and Dl (Figure 3G-I, P-R). These results revealed the causal relationship between stimulation of forebrain regions Dm and Dl with the activation of habenular neurons, thereby confirming functional connections from these ancestral limbic dorsal forebrain structures onto the habenula. Our results also demonstrated that structured ongoing activity of habenula carries information from its input regions in the forebrain.

Sensory information and limbic dorsal forebrain inputs are integrated in the habenula

Previous studies showed that habenular neurons receive direct inputs from the olfactory bulbs [38, 111] and exhibit prominent chemosensory responses to diverse odors [39, 53, 87, 130]. Our functional connectivity analysis (Figure 2) and forebrain micro-stimulation experiments (Figure 3) also showed that at least a part of the ongoing habenular activity is generated by the activity of the olfactory pathway and the limbic forebrain regions Dm and Dl. We asked how these chemosensory and non-sensory forebrain inputs are integrated at the level of habenula. To do this, we established a nose-attached intact brain-explant preparation [131, 132] of juvenile zebrafish, which allowed micro-electrode stimulation of limbic dorsal forebrain regions, while delivering odors to the nose (Figure 4A). We observed habenular responses both upon odor delivery and dorsal forebrain micro-electrode stimulation (Figure 4B, C). We tested whether the habenula has distinct populations of neurons with different preferences for dorsal forebrain and olfactory inputs. Interestingly, a majority of the habenular neurons that are strongly activated by the micro-stimulation of the dorsal forebrain showed weak or no odor responses (Figure 4E), supporting the idea that habenula is composed of distinct zones with sensory or limbic inputs. Next, we asked whether chemosensory and limbic inputs to habenula can influence each other, when they are delivered simultaneously (Figure 4D). We first visualized the influence of dorsal forebrain stimulation on the habenular odor responses, by plotting the odor responses of habenular neurons against the change of their odor responses in the presence of forebrain stimulation (Figure 4F). In fact, 18.3% of odor

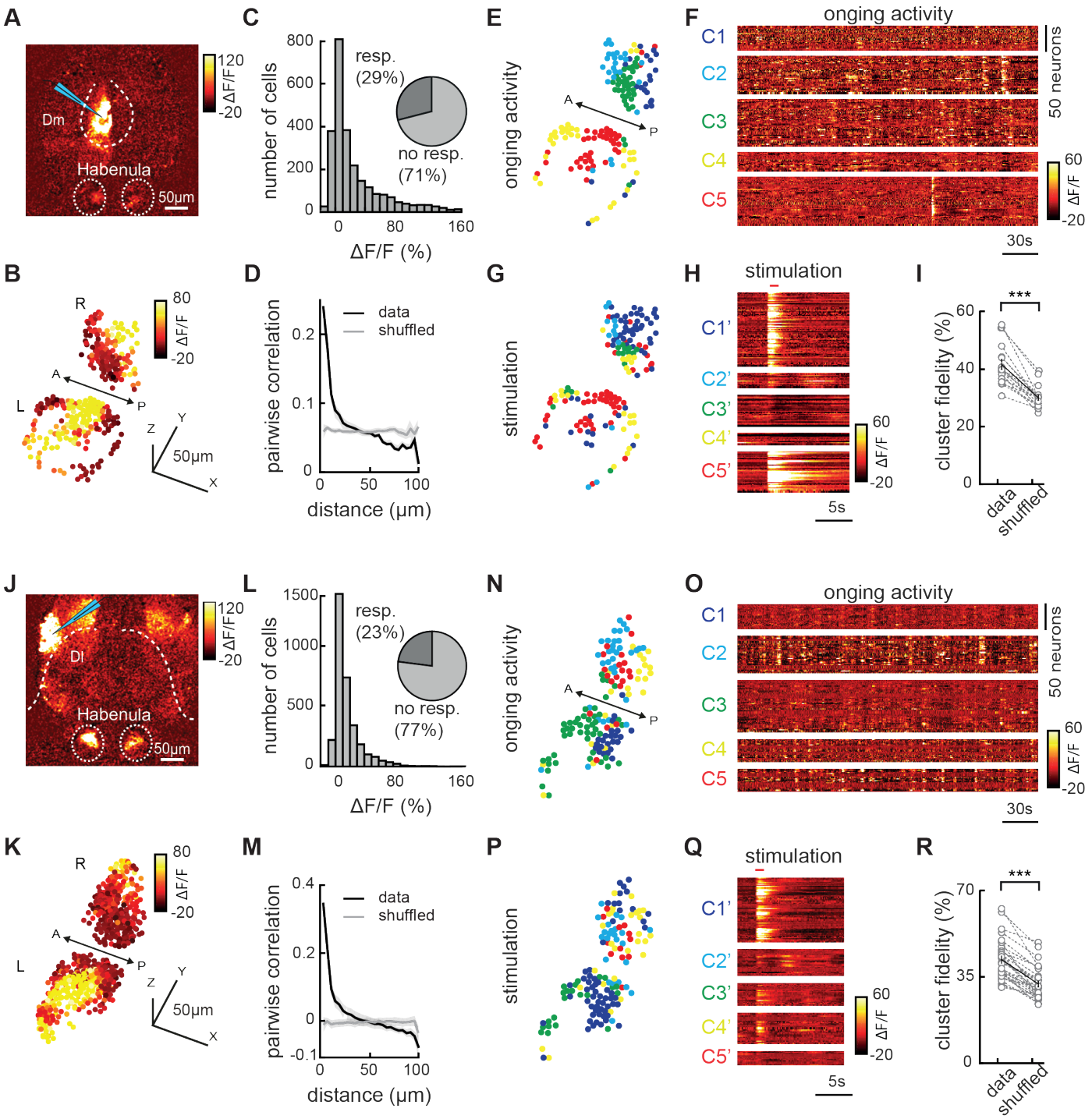

Figure 3: Electrical micro-stimulation of forebrain regions Dm and Dl activates spatially organized clusters of habenular neurons.

(A) Two-photon calcium signals upon electrical micro-stimulation of forebrain region Dm, in Tg(eval3:GCaMP5) juvenile zebrafish brain explant. Warm colors represent stronger neural activity. Cyan triangle represents electrode location. Habenula and Dm are delineated with dashed lines. (B) Reconstruction of habenular responses upon Dm micro-stimulation. (C) Histogram representing the responses of habenular neurons upon Dm micro-stimulation (511±72 neurons per fish, in n=5 fish). Pie-chart represents the ratio of habenular neurons that are activated 2 SDs higher than baseline levels, upon Dm micro-stimulation. (D) Relation between pairwise correlation of habenular neuron responses upon Dm micro-stimulation and the distance between each neuron pair. Grey line represents shuffled spatial distribution. (E) Reconstruction of habenular neurons clustered with k-means functional clustering of their ongoing activity in juvenile zebrafish brain explant. Colors represent habenular clusters with similar ongoing activity. Scale bar represents 50µm. L – left; R – right hemisphere. (F) Ongoing activity of the habenular neurons corresponding to clusters in E. (G) Reconstruction of habenular neurons clustered during Dm micro-stimulation using k-means clustering. Colors represent habenular clusters with similar responses to Dm micro-stimulation. L – left; R – right hemisphere. (H) Responses of habenular neurons upon Dm micro-stimulation clustered by k-means clustering. Forebrain micro-stimulations is marked in red. Warm colors represent higher neural activity. (I) The ratio of habenular neuron pairs remaining in the same functional clusters (high cluster fidelity) is significantly higher than chance levels, during ongoing activity and Dm micro-stimulation. ***p<0.001, Wilcoxon signed rank test. (J) Two-photon calcium signals upon electrical micro-stimulation of forebrain region Dl, in Tg(eval3:GCaMP5) juvenile zebrafish brain-explant.. Cyan triangle represents electrode location. Habenula and Dl are delineated with dashed lines. (K) Reconstruction

of habenular responses upon Dl micro-stimulation. (L) Histogram representing the responses of habenular neurons upon Dl micro-stimulation (575±92 neurons per fish, in n=6 fish). Pie-chart represents the ratio of habenular neurons that are activated 2 SDs higher then baseline levels upon Dl micro-stimulation. (M) Relation between pairwise correlation of habenular neuron responses upon Dl micro-stimulation and the distance between each neuron pair. Grey line represents shuffled spatial distribution. (N) Reconstruction of habenular neurons clustered with k-means functional clustering of their ongoing activity in juvenile zebrafish brain explant. Colors represent habenular clusters with similar ongoing activity. L-left; R-right hemisphere. (O) Ongoing activity of the habenular neurons corresponding to clusters in N. (P) Reconstruction of habenular neurons clustered during Dl micro-stimulation using k-means clustering. Colors represent habenular clusters with similar responses to Dl micro-stimulation. L – left; R – right hemisphere. (Q) Responses of habenular neurons upon Dl micro-stimulation clustered by k-means clustering. Forebrain micro-stimulations is marked in red. (R) The ratio of habenular neuron pairs remaining in the same functional clusters (high cluster fidelity) is significantly higher than chance levels, during ongoing activity and Dl micro-stimulation. ***p<0.001, Wilcoxon signed rank test.signed rank test.

responding habenular neurons showed a significant change in their odor responses upon forebrain stimulation (Figure 4F, black). The majority of these significantly modulated odor responses were weakly odor responding habenular neurons, whose responses were potentiated by forebrain stimulation. Next, we asked whether odor stimuli can modulate the responses of habenular neurons to forebrain stimulation. We observed that odor delivery significantly modulates forebrain driven responses in 21.7% of habenular neurons (Figure 4G, black), with a broad preference for inhibition of forebrain responses in the habenula, during odor stimulation (negative values in y axis, Figure 4G). These results indicate that the habenula integrates chemosensory and limbic information, and that these two different types of inputs can modulate

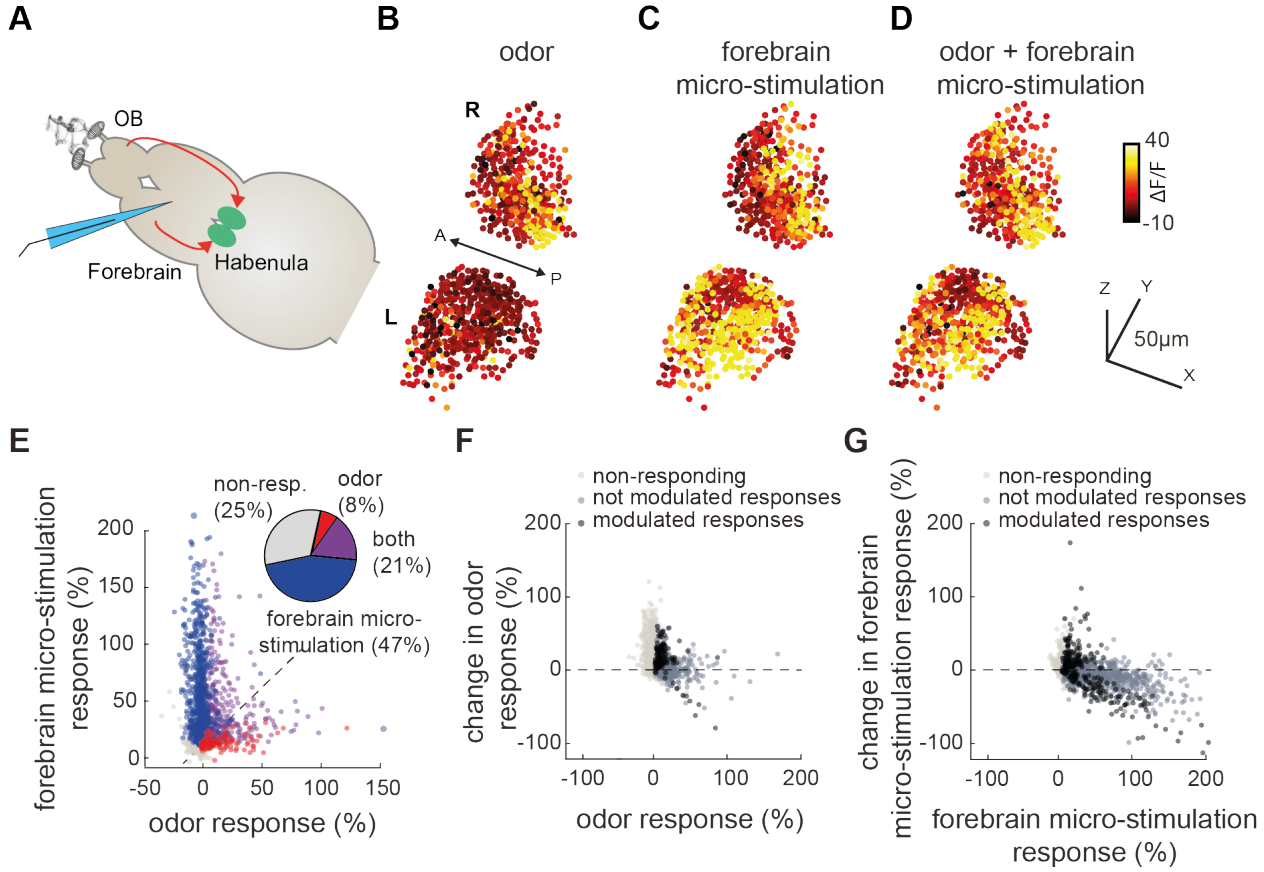

Figure 4: Habenular neurons integrate inputs from dorsal forebrain and olfactory system in a non-linear manner. (A) Schematic representation of nose-attached brain-explant preparation in Tg(elavl3:GCaMP6s) juvenile zebrafish, allowing simultaneous micro-stimulation of dorsal forebrain and odor stimulation of the nose. Habenula is marked in green, stimulation electrode is marked in cyan. Red arrows represent olfactory and dorsal forebrain inputs. (B) Three-dimensional reconstruction of habenular responses to odor stimulation averaged over 6 trials Warm colors indicate stronger neural responses. L – left; R – right hemisphere. (C) Reconstruction of habenular responses to dorsal forebrain micro-stimulation averaged over 6 trials. (D) Three-dimensional reconstruction of habenular responses to simultaneous odor stimulation and dorsal forebrain micro-stimulation averaged over 6 trials. (E) Responses of individual habenular neurons to odor stimulation and dorsal forebrain micro-stimulation from 2550 neurons measured in n=5 fish. Pie chart represents the ratio of habenular neurons responding 2 SDs above baseline levels to only odors (red), only micro-stimulation (blue) and both (magenta). (F) Change of odor responses in habenular neurons upon dorsal forebrain stimulation. Dark grey marks habenular neurons responding to odor stimulation. Black marks habenular neurons responding to odor stimulation and that are significantly (p<0.05, Wilcoxon signed rank test) modulated by forebrain micro-stimulation. (G) Change of habenular neuron responses to dorsal forebrain activation upon odor stimulation. Dark grey marks habenular neurons responding to dorsal forebrain micro-stimulation. Black marks habenular neurons responding to dorsal forebrain micro-stimulation and that are significantly (p<0.05, Wilcoxon signed rank test) modulated by the presentation of odors.

each other, with a prominent suppression of limbic inputs during odor stimulation.

Chemosensory stimulation modulates the ongoing activity of habenular neurons that are functionally coupled with limbic forebrain regions

Our results combining odor delivery with forebrain micro-stimulation in zebrafish brain-explant showed that chemosensory stimulation can modulate the activity of habenular neurons that receive forebrain inputs. We asked whether such odor-induced modulation of limbic forebrain-driven habenular neurons is present in vivo. To test this, we first identified the habenular neurons that are strongly (top 5%) inhibited (in blue) or excited (in red) by a range of attractive and aversive odors (Figure 5A, B), and calculated the average ongoing activity of these neurons (Figure 5C). Next, we identified the top 5% of forebrain neurons (Figure 5D), which are strongly correlated with the ongoing activity of habenular neurons that are either strongly inhibited or excited by odors. Finally, we determined how these forebrain neurons with strong correlations to odor modulated habenular neurons are distributed into distinct forebrain regions identified manually, as described in Figure 2F. Our results revealed that zebrafish homolog of hippocampus Dl, contains the largest number of neurons that are highly correlated with odor modulated habenular neurons (Figure 5E). In fact, Dl is the only brain region that contains neurons correlated with odor modulated habenular neurons (Figure 5E, blue and red labels) significantly more than the shuffled chance levels dictated by the size of individual regions (Figure 5E, dashed line). We did not observe any difference in the effect of aversive or attractive odors (Figure S5A, B). Our observations

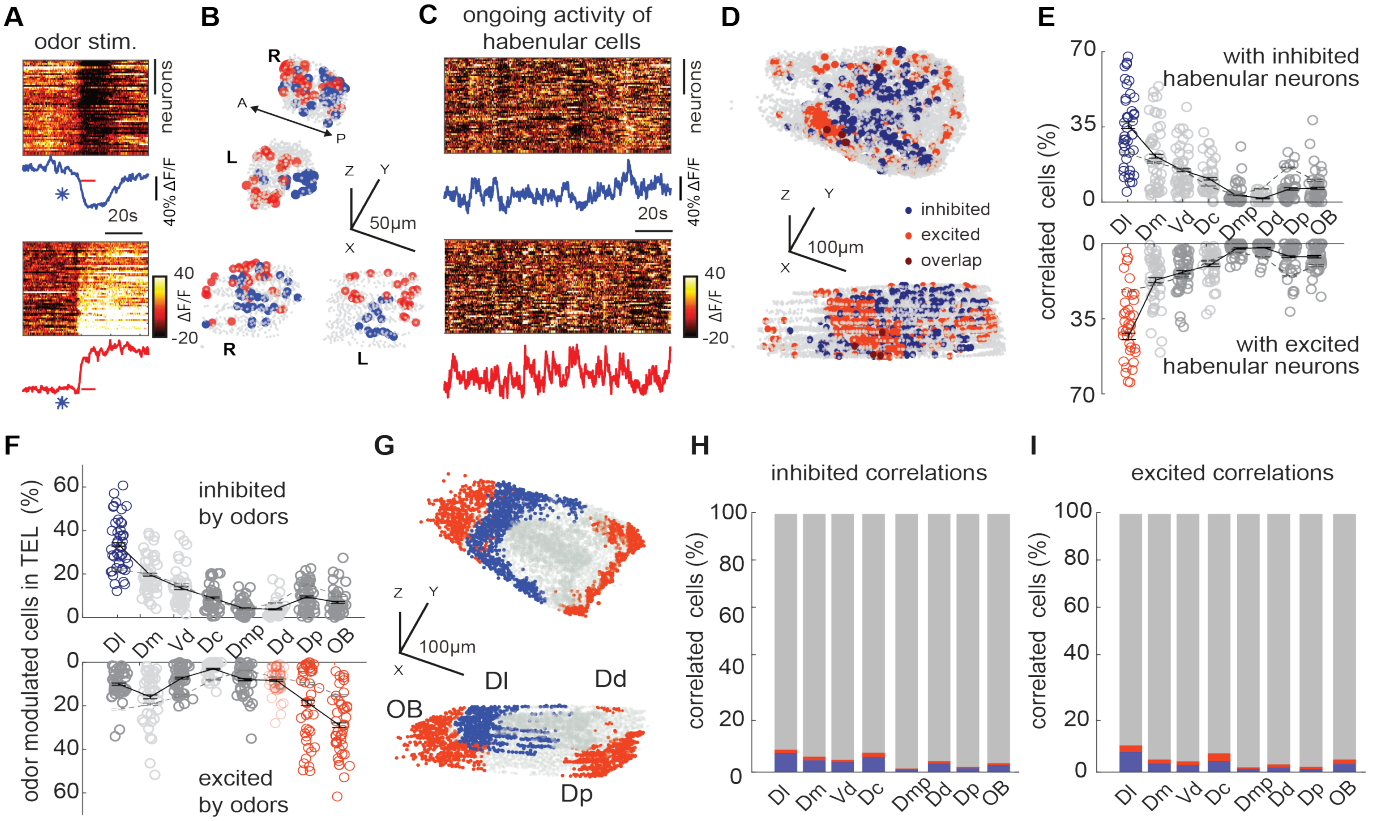

Figure 5: Odor-modulated habenular neurons are functionally connected with dorsal forebrain during ongoing activity. (A) Representative example of odor induced inhibition (top) and excitation (bottom) in habenular neurons of juvenile zebrafish. Dark colors represent inhibition (top 5% most inhibited neurons). Warm colors represent excitation (top 5% most excited neurons). Individual traces represent average inhibition (blue) and excitation (red) of habenular neurons. "*" indicates opening of odor valve, red bar indicates odor presentation. (B) Representative example of top 5% odor inhibited (blue) and excited (red) habenular neurons from an individual fish. 916 ± 39 (mean ± SEM) habenular neurons were imaged in each fish (n=10). (C) Ongoing neural activity of odor inhibited (top) and odor excited (bottom) habenular neurons in B. Lines represents the average activity of odor-inhibited (blue) and odor-excited (red) habenular neurons. (D) Representative example of top 5% forebrain neurons that are correlated with the ongoing activity of odor-inhibited (blue) and odor-excited (red) habenular neurons. 5799 ± 165 (mean ± SEM) forebrain neurons were imaged in each fish (n=10). (E) Anatomical distribution of forebrain neurons with strong correlations (top 5%) to ongoing activity of habenular neurons that are inhibited (top) and excited (bottom) by odors. Red and blue colored circles highlight forebrain regions that exhibit significantly higher synchrony to habenula than the chance levels dictated by the size of individual regions, $p < 0.01$, Wilcoxon signed-rank test. Black lines represent mean ± SEM. (F) Anatomical distribution of forebrain neurons that are most (top 5%) inhibited (top) and most excited (bottom) by odors. Colored circles highlight those forebrain regions that exhibit significantly higher number of odor-inhibited (blue) and odor-excited (red) neurons than the shuffled chance levels dictated by the size of individual regions, $p < 0.01$, Wilcoxon signed-rank test. Black lines represent mean ± SEM. (G) Representation of forebrain regions that show significantly higher number of odor-inhibited (blue) and odor-excited (red) neurons than the chance levels dictated by the size of individual regions. (H-I) Overlap of odor responding (blue: inhibited, red: excited) forebrain neurons and those forebrain neurons driving odor-inhibited (H) and odor-excited (I) habenular neurons.

were also robust at different thresholds for selecting forebrain neurons strongly correlated with odor-modulated habenular neurons (Figure S5C, D).

Our results demonstrate the presence of strong chemosensory modulation (excitation/inhibition) of limbic-driven habenular activity. Yet, it is not clear if such chemosensory modulation happens at the level of habenular neurons or also at the level of limbic forebrain regions of zebrafish. To investigate the distribution of chemosensory modulation of dorsal forebrain neurons, we determined odor responses across the forebrain. Our results showed that Dl is the only forebrain region with odor-inhibited neurons significantly above chance levels (Figure 5F, top). As expected, olfactory bulb and olfactory cortex (Dp) [133], have the largest fraction of odor excited neurons, that are also significantly above the chance levels, in addition to dorsal zone of dorsal telencephalon (Dd) (Figure 5F, bottom). We observed no significant differences in the distribution of attractive or aversive odor responses (Figure S5C, D). The locations of forebrain regions that are strongly (top 5%) inhibited (blue) or excited (red) by odors are highlighted in Figure 5G.

Next, we asked how much of this odor-induced excitation and inhibition across the forebrain can explain the odor modulation of habenular activity. We observed that only a small fraction (less than 10%) of odor-excited or -inhibited forebrain neurons, overlap with forebrain neurons that drive odor-modulated habenular neurons (Figure 5H, I). This finding suggests that odors can separately modulate the limbic forebrain and habenular neurons with limited functional connections. Altogether, our results revealed that odors inhibit the activity of the ancestral limbic forebrain circuits in zebrafish. We also showed that odor-induced modulation of habenular activity cannot solely be explained by the odor responses of forebrain neurons. These findings suggest that odor stimulation not only alters the dynamics of the forebrain circuitry but also changes the way habenula integrate its forebrain inputs, and further modulates the state of ongoing habenular activity.

DISCUSSION

In this study, we revealed the forebrain circuitry underlying ongoing habenular activity and showed that this inter-connected network can generate structured ongoing activity with strong synchrony and anti-synchrony that is stable over time. Our results further showed that chemosensory stimuli can modulate brain activity not only by activating the olfactory pathway, but also by suppressing the ongoing activity of habenular networks and its input regions in the forebrain that are ancestral to mammalian limbic system. Interestingly, our micro-stimulation experiments also revealed that the specific communication between habenula and its forebrain inputs is dampened in the presence of odor stimulation. Disruption of ongoing (or resting state) brain activity with sensory stimuli has also been observed in human subjects [3, 6, 7], suggesting a high-level of evolutionary conservation (or convergent evolution) of vertebrate brain dynamics and the way they interact with the sensory world. Such interactions could serve multiple purposes. First, disruption of ongoing or resting brain state with a salient sensory stimulus, can facilitate state transitions, when an animal needs to quickly attend, adapt and respond to salient environmental changes. In fact, such a role of the habenula in behavioral flexibility and in adapting to new conditions has been demonstrated in both zebrafish [8, 64, 65, 72, 73, 76] and mammals [1, 134, 135]. Second, dampening of ongoing habenular and forebrain activity might increase the sensitivity of these networks to incoming sensory information by reducing background noise levels. This would, in turn, increase the robustness of sensory representations to incoming stimuli following first encounter, as it is often the case with olfactory stimuli that are received by repeated exposure to odor plumes [136-138]. Finally, resetting the ongoing activity of limbic forebrain networks, might be an important mechanism allowing animals to make new associations, when conditions are altered, as it has been shown during reversal learning [1, 75, 78, 135]. How does the ongoing activity of these networks adapt during behavioral plasticity and learning will require well-established behavioral assays and simultaneous imaging of forebrain and habenular activity in juvenile zebrafish, that can perform cognitively demanding learning tasks [75, 95-97]. Moreover, given the multi-sensory responses of habenular circuits [52], it will also be interesting to test whether such interactions between sensory stimuli and ongoing brain activity generalize to other sensory modalities (e.g. vision, auditory), in future studies.

Anatomical projections from the olfactory bulb [38, 111], entopeduncular nucleus [41, 49, 55, 58], and lateral hypothalamus [41, 47, 100] to habenula have been shown by several past studies. In addition to these anatomically confirmed regions, our results showed that Dl and Dm, zebrafish homologs of mammalian hippocampus and amygdala, are the main dorsal forebrain regions that are strongly correlated with ongoing habenular activity. We also confirmed these functional connectivity measures based on correlations, by further micro- stimulation of Dl and Dm that activate up to ~30% of habenular neurons. It is yet to be discovered whether distinct habenular sub-circuits encode information from different forebrain regions. To our knowledge no direct anatomical projections from Dl or Dm were reported to innervate habenula in zebrafish. Nevertheless, Dm neurons were shown to innervate entopeduncular nucleus and hypothalamus [106] both of which were shown to

project to habenula in zebrafish and mammals [41, 47, 56, 58, 100, 102, 125, 128]. Dl neurons are a larger group of neurons, which are likely functionally heterogenous due to large size of Dl region. All studies of Dl in teleost fish highlight a homology of this structure with hippocampal-entorhinal circuitry related to episodic memory and spatial navigation [119, 120, 123, 126, 139]. In fact, similar to our findings in zebrafish, functional coupling between hippocampal circuitry and habenula has been shown also in rodents [140-142]. All these results suggest that there might be direct or indirect connections from hippocampal circuitry to habenula. Extensive anatomical reconstructions of Dl neurons, by using newly generated electron- and light- microscopy imaging data sets from zebrafish brains [105, 143], will shed more light onto direct or multi-synaptic anatomical connections between the habenula and the hippocampal system. This may also highlight new avenues of research on the role of habenula for episodic memories and spatial navigation.

As a small vertebrate, zebrafish exhibit general principles of vertebrate forebrain architecture. Most studies of zebrafish forebrain circuitry have investigated adult zebrafish with sophisticated behaviors and large brains that are challenging to access using optical imaging methods and requires surgery [125, 144, 145]. The forebrain, especially the dorsal telencephalon, of transparent 5-10 days old zebrafish larvae is not yet fully developed [52, 128, 146]. Hence, using 3 to 4-week-old juvenile zebrafish provides an alternative approach to study a relatively developed forebrain network [52, 128, 146] that is still optically accessible to imaging the entire forebrain, including habenula, as we demonstrated in this study. This approach allowed us to identify functionally distinct populations of forebrain neurons, which also overlapped with distinct forebrain regions that we could identify based on anatomical landmarks. Our calcium imaging results allowed us to relate some of these functionally defined zones in juvenile zebrafish forebrain with adult zebrafish, other teleosts and even mammalian forebrain structures. Given the ability of juvenile zebrafish to perform cognitively demanding behaviors such as social interactions [97, 98] and learning [75, 95, 96], while allowing non-invasive functional imaging, we hope that future studies will shed further light onto the function and the connectivity of forebrain networks during these behaviors.

Altogether our results highlight the activity and connectivity of forebrain networks underlying ongoing habenular activity and revealed how habenula integrates olfactory and limbic information. Our findings further support the idea that the habenula serve as a main hub [44, 74], which can integrate sensory and non-sensory information from diverse forebrain regions and relays this integrated information to its downstream targets regulating animal behavior [41, 43-48, 50, 58]. Given the important role of habenula in adaptive behaviours and mood disorders [147-150], our results suggest that sensory experience might provide a non-invasive pathway to modulate habenular activity, perhaps also in humans. Future studies with high-throughput and high-resolution brain imaging methods in mammals, may answer whether sensory information can perturb the dynamics of ongoing activity of mammalian habenula.

ACKNOWLEDGEMENTS

We thank M. Ahrens (HHMI, Janelia Farm, USA), K. Kawakami (National Institute of Genetics, Japan) for transgenic lines. We thank S. Eggen, M. Andresen, V. Nguyen and our fish facility support team for technical assistance. We thank the Yaksi lab members for stimulating discussions. We thank Steffen Kandler and Nathalie Jurisch-Yaksi for their feedback on the manuscript. This work was funded by ERC starting grant 335561 (E.Y.), Helse Midt-Norge Samarbeidsorganet grant (E.Y.), RCN FRIPRO Research Grant 239973 (E.Y.), Boehringer Ingelheim Fonds (S.K.J.). Work in the E.Y. lab is funded by the Kavli Institute for Systems Neuroscience at NTNU.

AUTHOR CONTRIBUTIONS

Conceptualization, E.M.B., S.K.J., E.Y.; Methodology and data, E.M.B., S.K.J., E.Y.; Data Analysis, E.M.B., S.K.J., K.T.P.C., E.Y.; Investigation, all authors; Writing, E.M.B., E.Y.; Review & Editing, all authors; Funding Acquisition and Supervision, E.Y.

DECLARATION OF INTERESTS

The authors declare no competing interests.

REFERENCES

1. Baker, P.M., Oh, S.E., Kidder, K.S., and Mizumori, S.J. (2015). Ongoing behavioral state information signaled in the lateral habenula guides choice flexibility in freely moving rats. Front Behav Neurosci 9, 295.

2. McAdams, C.J., and Reid, R.C. (2005). Attention modulates the responses of simple cells in monkey primary visual cortex. J Neurosci 25, 11023-11033.

3. Raichle, M.E., MacLeod, A.M., Snyder, A.Z., Powers, W.J., Gusnard, D.A., and Shulman, G.L. (2001). A default mode of brain function. P Natl Acad Sci USA 98, 676-682.

4. Buckner, R.L., Andrews-Hanna, J.R., and Schacter, D.L. (2008). The brain's default network: anatomy, function, and relevance to disease. Ann N Y Acad Sci 1124, 1-38.

5. Raichle, M.E. (2015). The Brain's Default Mode Network. Annu Rev Neurosci 38, 433-447.

6. Greicius, M.D., and Menon, V. (2004). Default-mode activity during a passive sensory task: Uncoupled from deactivation but impacting activation. J Cognitive Neurosci 16, 1484-1492.

7. Shulman, G.L., Fiez, J.A., Corbetta, M., Buckner, R.L., Miezin, F.M., Raichle, M.E., and Petersen, S.E. (1997). Common blood flow changes across visual tasks .2. Decreases

in cerebral cortex. J Cognitive Neurosci 9, 648-663.
8. Andalman, A.S., Burns, V.M., Lovett-Barron, M., Broxton, M., Poole, B., Yang, S.J., Grosenick, L., Lerner, T.N., Chen, R., Benster, T., et al. (2019). Neuronal Dynamics Regulating Brain and Behavioral State Transitions. Cell 177, 970-985 e920.
9. Fox, M.D., Snyder, A.Z., Vincent, J.L., Corbetta, M., Van Essen, D.C., and Raichle, M.E. (2005). The human brain is intrinsically organized into dynamic, anticorrelated functional networks. P Natl Acad Sci USA 102, 9673-9678.
10. Lovett-Barron, M., Andalman, A.S., Allen, W.E., Vesuna, S., Kauvar, I., Burns, V.M., and Deisseroth, K. (2017). Ancestral Circuits for the Coordinated Modulation of Brain State. Cell 171, 1411-+.
11. Marques, J.C., Li, M., Schaak, D., Robson, D.N., and Li, J.M. (2020). Internal state dynamics shape brainwide activity and foraging behaviour. Nature 577, 239-243.
12. Musall, S., Kaufman, M.T., Juavinett, A.L., Gluf, S., and Churchland, A.K. (2019). Single-trial neural dynamics are dominated by richly varied movements. Nat Neurosci 22, 1677-+.
13. Shimaoka, D., Steinmetz, N.A., Harris, K.D., and Carandini, M. (2019). The impact of bilateral ongoing activity on evoked responses in mouse cortex. Elife 8.
14. Stringer, C., Pachitariu, M., Steinmetz, N., Reddy, C.B., Carandini, M., and Harris, K.D. (2019). Spontaneous behaviors drive multidimensional, brainwide activity. Science 364, 255-+.
15. Bianco, I.H., and Engert, F. (2015). Visuomotor Transformations Underlying Hunting Behavior in Zebrafish. Curr Biol 25, 831-846.
16. Arieli, A., Sterkin, A., Grinvald, A., and Aertsen, A. (1996). Dynamics of ongoing activity: explanation of the large variability in evoked cortical responses. Science 273, 1868-1871.
17. Nauhaus, I., Busse, L., Carandini, M., and Ringach, D.L. (2009). Stimulus contrast modulates functional connectivity in visual cortex. Nat Neurosci 12, 70-76.
18. Romano, S.A., Pietri, T., Perez-Schuster, V., Jouary, A., Haudrechy, M., and Sumbre, G. (2015). Spontaneous Neuronal Network Dynamics Reveal Circuit's Functional Adaptations for Behavior. Neuron 85, 1070-1085.
19. Tsitoura, C., Malinowski, S.T., Mohrhardt, J., Degen, R., DiBenedictis, B.T., Gao, Y., Watznauer, K., Gerhold, K., Nagel, M., Weber, M., et al. (2020). Synchronous Infra-Slow Oscillations Organize Ensembles of Accessory Olfactory Bulb Projection Neurons into Distinct Microcircuits. J Neurosci 40, 4203-4218.
20. Fdez Galan, R., Sachse, S., Galizia, C.G., and Herz, A.V. (2004). Odor-driven attractor dynamics in the antennal lobe allow for simple and rapid olfactory pattern classification. Neural Comput 16, 999-1012.
21. Gretenkord, S., Kostka, J.K., Hartung, H., Watznauer, K., Fleck, D., Minier-Toribio, A., Spehr, M., and Hanganu-Opatz, I.L. (2019). Coordinated electrical activity in the olfactory bulb gates the oscillatory entrainment of entorhinal networks in neonatal mice. PLoS Biol 17, e2006994.
22. Galan, R.F., Weidert, M., Menzel, R., Herz, A.V.M., and Galizia, C.G. (2006). Sensory memory for odors is encoded in spontaneous correlated activity between olfactory glomeruli. Neural Computation 18, 10-25.
23. Eggermont, J.J. (2015). Animal models of spontaneous activity in the healthy and impaired auditory system. Front Neural Circuit 9.
24. Kullmann, S., Heni, M., Linder, K., Zipfel, S., Haring, H.U., Veit, R., Fritsche, A., and Preissl, H. (2014). Resting-State Functional Connectivity of the Human Hypothalamus. Hum Brain Mapp 35, 6088-6096.
25. Bashore, T.R., Rebec, G.V., and Groves, P.M. (1978). Alterations of Spontaneous Neuronal-Activity in Caudate-Putamen, Nucleus Accumbens and Amygdaloid Complex of Rats Produced by D-Amphetamine. Pharmacol Biochem Be 8, 467-474.
26. Luo, Y.J., Li, Y.D., Wang, L., Yang, S.R., Yuan, X.S., Wang, J., Cherasse, Y., Lazarus, M., Chen, J.F., Qu, W.M., et al. (2018). Nucleus accumbens controls wakefulness by a subpopulation of neurons expressing dopamine D-1 receptors. Nat Commun 9.
27. Hosomi, F., Yanagi, M., Kawakubo, Y., Tsujii, N., Ozaki, S., and Shirakawa, O. (2019). Capturing spontaneous activity in the medial prefrontal cortex using near-infrared spectroscopy and its application to schizophrenia. Sci Rep-Uk 9.
28. Yanagi, M., Hosomi, F., Kawakubo, Y., Tsuchiya, A., Ozaki, S., and Shirakawa, O. (2020). A decrease in spontaneous activity in medial prefrontal cortex is associated with sustained hallucinations in chronic schizophrenia: An NIRS study. Sci Rep-Uk 10.
29. Hahn, T.T.G., McFarland, J.M., Berberich, S., Sakmann, B., and Mehta, M.R. (2012). Spontaneous persistent activity in entorhinal cortex modulates cortico-hippocampal interaction in vivo. Nat Neurosci 15, 1531-1538.
30. Valeeva, G., Janackova, S., Nasretdinov, A., Rychkova, V., Makarov, R., Holmes, G.L., Khazipov, R., and Lenck-Santini, P.P. (2019). Emergence of Coordinated Activity in the Developing Entorhinal-Hippocampal Network. Cereb Cortex 29, 906-920.
31. Long, J.Y., Luo, L.K., Guo, Y., You, W.F., Li, Q., Li, B., Tang, W.J., Yang, Y.C., Kemp, G.J., Sweeney, J.A., et al. (2020). Altered spontaneous activity and effective connectivity of the anterior cingulate cortex in obsessive-compulsive disorder. J Comp Neurol.
32. Sellmeijer, J., Mathis, V., Hugel, S., Li, X.H., Song, Q., Chen, Q.Y., Barthas, F., Lutz, P.E., Karatas, M., Luthi, A., et al. (2018). Hyperactivity of Anterior Cingulate Cortex Areas 24a/24b Drives Chronic Pain-Induced Anxiodepressive-like Consequences. J Neurosci 38, 3102-3115.
33. Yague, J.G., Tsunematsu, T., and Sakata, S. (2017). Distinct Temporal Coordination of Spontaneous Population Activity between Basal Forebrain and Auditory Cortex. Front Neural Circuit 11.
34. Koyama, S., Kanemitsu, Y., and Weight, F.F. (2005). Spontaneous activity and properties of two types of principal neurons from the ventral tegmental area of rat. J Neurophysiol 93, 3282-3293.
35. Khaliq, Z.M., and Bean, B.P. (2010). Pacemaking in Dopaminergic Ventral Tegmental Area Neurons: Depolarizing Drive from Background and Voltage-Dependent Sodium Conductances. J Neurosci 30, 7401-7413.
36. Chan, V., Starr, P.A., and Turner, R.S. (2011). Bursts

and oscillations as independent properties of neural activity in the parkinsonian globus pallidus internus. Neurobiol Dis 41, 2-10.
37. Weis, C.N., Huggins, A.A., Bennett, K.P., Parisi, E.A., and Larson, C.L. (2019). High-Resolution Resting-State Functional Connectivity of the Extended Amygdala. Brain Connect 9, 627-637.
38. Miyasaka, N., Morimoto, K., Tsubokawa, T., Higashijima, S., Okamoto, H., and Yoshihara, Y. (2009). From the olfactory bulb to higher brain centers: genetic visualization of secondary olfactory pathways in zebrafish. J Neurosci 29, 4756-4767.
39. Cheng, R.K., Krishnan, S., Lin, Q., Kibat, C., and Jesuthasan, S. (2017). Characterization of a thalamic nucleus mediating habenula responses to changes in ambient illumination. BMC Biol 15, 104.
40. Zhang, B.B., Yao, Y.Y., Zhang, H.F., Kawakami, K., and Du, J.L. (2017). Left Habenula Mediates Light-Preference Behavior in Zebrafish via an Asymmetrical Visual Pathway. Neuron 93, 914-928 e914.
41. Turner, K.J., Hawkins, T.A., Yanez, J., Anadon, R., Wilson, S.W., and Folgueira, M. (2016). Afferent Connectivity of the Zebrafish Habenulae. Front Neural Circuits 10, 30.
42. Lecca, S., Pelosi, A., Tchenio, A., Moutkine, I., Lujan, R., Herve, D., and Mameli, M. (2016). Rescue of GABA(B) and GIRK function in the lateral habenula by protein phosphatase 2A inhibition ameliorates depression-like phenotypes in mice. Nat Med 22, 254-261.
43. Warden, M.R., Selimbeyoglu, A., Mirzabekov, J.J., Lo, M., Thompson, K.R., Kim, S.Y., Adhikari, A., Tye, K.M., Frank, L.M., and Deisseroth, K. (2012). A prefrontal cortex-brainstem neuronal projection that controls response to behavioural challenge. Nature 492, 428-432.
44. Okamoto, H., Agetsuma, M., and Aizawa, H. (2012). Genetic dissection of the zebrafish habenula, a possible switching board for selection of behavioral strategy to cope with fear and anxiety. Dev Neurobiol 72, 386-394.
45. Matsumoto, M., and Hikosaka, O. (2007). Lateral habenula as a source of negative reward signals in dopamine neurons. Nature 447, 1111-1115.
46. Meye, F.J., Soiza-Reilly, M., Smit, T., Diana, M.A., Schwarz, M.K., and Mameli, M. (2016). Shifted pallidal co-release of GABA and glutamate in habenula drives cocaine withdrawal and relapse. Nat Neurosci 19, 1019-1024.
47. Lazaridis, I., Tzortzi, O., Weglage, M., Martin, A., Xuan, Y., Parent, M., Johansson, Y., Fuzik, J., Furth, D., Fenno, L.E., et al. (2019). A hypothalamus-habenula circuit controls aversion. Mol Psychiatry.
48. Stamatakis, A.M., Jennings, J.H., Ung, R.L., Blair, G.A., Weinberg, R.J., Neve, R.L., Boyce, F., Mattis, J., Ramakrishnan, C., Deisseroth, K., et al. (2013). A unique population of ventral tegmental area neurons inhibits the lateral habenula to promote reward. Neuron 80, 1039-1053.
49. Hong, S., Jhou, T.C., Smith, M., Saleem, K.S., and Hikosaka, O. (2011). Negative reward signals from the lateral habenula to dopamine neurons are mediated by rostromedial tegmental nucleus in primates. J Neurosci 31, 11457-11471.
50. Herkenham, M., and Nauta, W.J. (1977). Afferent connections of the habenular nuclei in the rat. A horseradish peroxidase study, with a note on the fiber-of-passage problem. J Comp Neurol 173, 123-146.
51. Ambrosi, E., Arciniegas, D.B., Curtis, K.N., Patriquin, M.A., Spalletta, G., Sani, G., Frueh, B.C., Fowler, J.C., Madan, A., and Salas, R. (2019). Resting-State Functional Connectivity of the Habenula in Mood Disorder Patients With and Without Suicide-Related Behaviors. J Neuropsych Clin N 31, 49-56.
52. Fore, S., Acuna-Hinrichsen, F., Mutlu, K.A., Bartoszek, E.M., Serneels, B., Faturos, N.G., Chau, K.T.P., Cosacak, M.I., Verdugo, C.D., Palumbo, F., et al. (2020). Functional properties of habenular neurons are determined by developmental stage and sequential neurogenesis. Sci Adv 6.
53. Jetti, S.K., Vendrell-Llopis, N., and Yaksi, E. (2014). Spontaneous activity governs olfactory representations in spatially organized habenular microcircuits. Curr Biol 24, 434-439.
54. Yang, Y., Cui, Y., Sang, K., Dong, Y., Ni, Z., Ma, S., and Hu, H. (2018). Ketamine blocks bursting in the lateral habenula to rapidly relieve depression. Nature 554, 317-322.
55. Stephenson-Jones, M., Floros, O., Robertson, B., and Grillner, S. (2012). Evolutionary conservation of the habenular nuclei and their circuitry controlling the dopamine and 5-hydroxytryptophan (5-HT) systems. P Natl Acad Sci USA 109, E164-E173.
56. Bromberg-Martin, E.S., Matsumoto, M., Hong, S., and Hikosaka, O. (2010). A pallidus-habenula-dopamine pathway signals inferred stimulus values. J Neurophysiol 104, 1068-1076.
57. Bianco, I.H., and Wilson, S.W., (2009). The Habenula nuclei: a conserved asymmetric relay station in the vertebrate brain. Philos. Trans. R. Soc. B Biol. Sci. 364, 1005-1020.
58. Hendricks, M., and Jesuthasan, S. (2007). Asymmetric innervation of the habenula in zebrafish. J Comp Neurol 502, 611-619.
59. Nishikawa, T., Fage, D., and Scatton, B. (1986). Evidence for, and Nature of, the Tonic Inhibitory Influence of Habenulointerpeduncular Pathways Upon Cerebral Dopaminergic Transmission in the Rat. Brain Res 373, 324-336.
60. Root, D.H., Mejias-Aponte, C.A., Qi, J., and Morales, M. (2014). Role of glutamatergic projections from ventral tegmental area to lateral habenula in aversive conditioning. J Neurosci 34, 13906-13910.
61. Bernard, R., and Veh, R.W. (2012). Individual neurons in the rat lateral habenular complex project mostly to the dopaminergic ventral tegmental area or to the serotonergic raphe nuclei. J Comp Neurol 520, 2545-2558.
62. Hong, E., Santhakumar, K., Akitake, C.A., Ahn, S.J., Thisse, C., Thisse, B., Wyart, C., Mangin, J.M., and Halpern, M.E. (2013). Cholinergic left-right asymmetry in the habenulo-interpeduncular pathway. Proc Natl Acad Sci U S A 110, 21171-21176.
63. McLaughlin, I., Dani, J.A., and De Biasi, M. (2017). The medial habenula and interpeduncular nucleus circuitry is critical in addiction, anxiety, and mood regulation. J Neurochem 142 Suppl 2, 130-143.
64. Amo, R., Fredes, F., Kinoshita, M., Aoki, R., Aizawa, H., Agetsuma, M., Aoki, T., Shiraki, T., Kakinuma, H., Matsuda, M., et al. (2014). The habenulo-raphe serotonergic circuit encodes an aversive expectation value essential for adaptive

active avoidance of danger. Neuron 84, 1034-1048.
65. Duboue, E.R., Hong, E., Eldred, K.C., and Halpern, M.E. (2017). Left Habenular Activity Attenuates Fear Responses in Larval Zebrafish. Curr Biol 27, 2154-2162 e2153.
66. Krishnan, S., Mathuru, A.S., Kibat, C., Rahman, M., Lupton, C.E., Stewart, J., Claridge-Chang, A., Yen, S.C., and Jesuthasan, S. (2014). The right dorsal habenula limits attraction to an odor in zebrafish. Curr Biol 24, 1167-1175.
67. Lin, Q., and Jesuthasan, S. (2017). Masking of a circadian behavior in larval zebrafish involves the thalamo-habenula pathway. Sci Rep 7, 4104.
68. Hikosaka, O. (2010). The habenula: from stress evasion to value-based decision-making. Nat Rev Neurosci 11, 503-513.
69. Flanigan, M., Aleyasin, H., Takahashi, A., Golden, S.A., and Russo, S.J. (2017). An emerging role for the lateral habenula in aggressive behavior. Pharmacol Biochem Behav 162, 79-86.
70. Baker, P.M., Raynor, S.A., Francis, N.T., and Mizumori, S.J. (2017). Lateral habenula integration of proactive and retroactive information mediates behavioral flexibility. Neuroscience 345, 89-98.
71. Kawai, T., Yamada, H., Sato, N., Takada, M., and Matsumoto, M. (2015). Roles of the Lateral Habenula and Anterior Cingulate Cortex in Negative Outcome Monitoring and Behavioral Adjustment in Nonhuman Primates. Neuron 88, 792-804.
72. Chou, M.Y., Amo, R., Kinoshita, M., Cherng, B.W., Shimazaki, H., Agetsuma, M., Shiraki, T., Aoki, T., Takahoko, M., Yamazaki, M., et al. (2016). Social conflict resolution regulated by two dorsal habenular subregions in zebrafish. Science 352, 87-90.
73. Agetsuma, M., Aizawa, H., Aoki, T., Nakayama, R., Takahoko, M., Goto, M., Sassa, T., Amo, R., Shiraki, T., Kawakami, K., et al. (2010). The habenula is crucial for experience-dependent modification of fear responses in zebrafish. Nat Neurosci 13, 1354-1356.
74. Fore, S., Palumbo, F., Pelgrims, R., and Yaksi, E. (2018). Information processing in the vertebrate habenula. Semin Cell Dev Biol 78, 130-139.
75. Palumbo, F., Serneels, B., Pelgrims, R., and Yaksi, E. (2020). The Zebrafish Dorsolateral Habenula Is Required for Updating Learned Behaviors. Cell Rep 32.
76. Lee, A., Mathuru, A.S., Teh, C., Kibat, C., Korzh, V., Penney, T.B., and Jesuthasan, S. (2010). The habenula prevents helpless behavior in larval zebrafish. Curr Biol 20, 2211-2216.
77. Trusel, M., Nuno-Perez, A., Lecca, S., Harada, H., Lalive, A.L., Congiu, M., Takemoto, K., Takahashi, T., Ferraguti, F., and Mameli, M. (2019). Punishment-Predictive Cues Guide Avoidance through Potentiation of Hypothalamus-to-Habenula Synapses. Neuron 102, 120-127 e124.
78. Cherng, B.W., Islam, T., Torigoe, M., Tsuboi, T., and Okamoto, H. (2020). The Dorsal Lateral Habenula-Interpeduncular Nucleus Pathway Is Essential for Left-Right-Dependent Decision Making in Zebrafish. Cell Rep 32, 108143.
79. Huang, L., Xi, Y., Peng, Y., Yang, Y., Huang, X., Fu, Y., Tao, Q., Xiao, J., Yuan, T., An, K., et al. (2019). A Visual Circuit Related to Habenula Underlies the Antidepressive Effects of Light Therapy. Neuron.
80. Aizawa, H., Kobayashi, M., Tanaka, S., Fukai, T., and Okamoto, H. (2012). Molecular characterization of the subnuclei in rat habenula. J Comp Neurol 520, 4051-4066.
81. deCarvalho, T.N., Subedi, A., Rock, J., Harfe, B.D., Thisse, C., Thisse, B., Halpern, M.E., and Hong, E. (2014). Neurotransmitter map of the asymmetric dorsal habenular nuclei of zebrafish. Genesis 52, 636-655.
82. Viswanath, H., Carter, A.Q., Baldwin, P.R., Molfese, D.L., and Salas, R. (2013). The medial habenula: still neglected. Front Hum Neurosci 7, 931.
83. Pandey, S., Shekhar, K., Regev, A., and Schier, A.F. (2018). Comprehensive Identification and Spatial Mapping of Habenular Neuronal Types Using Single-Cell RNA-Seq. Curr Biol 28, 1052-1065 e1057.
84. Seigneur, E., Polepalli, J.S., and Sudhof, T.C. (2018). Cbln2 and Cbln4 are expressed in distinct medial habenula-interpeduncular projections and contribute to different behavioral outputs. Proc Natl Acad Sci U S A 115, E10235-E10244.
85. Ren, J., Qin, C., Hu, F., Tan, J., Qiu, L., Zhao, S., Feng, G., and Luo, M. (2011). Habenula "cholinergic" neurons co-release glutamate and acetylcholine and activate postsynaptic neurons via distinct transmission modes. Neuron 69, 445-452.
86. Amo, R., Aizawa, H., Takahoko, M., Kobayashi, M., Takahashi, R., Aoki, T., and Okamoto, H. (2010). Identification of the zebrafish ventral habenula as a homolog of the mammalian lateral habenula. J Neurosci 30, 1566-1574.
87. Dreosti, E., Vendrell Llopis, N., Carl, M., Yaksi, E., and Wilson, S.W. (2014). Left-right asymmetry is required for the habenulae to respond to both visual and olfactory stimuli. Curr Biol 24, 440-445.
88. Bromberg-Martin, E.S., Matsumoto, M., Nakahara, H., and Hikosaka, O. (2010). Multiple timescales of memory in lateral habenula and dopamine neurons. Neuron 67, 499-510.
89. Lupton, C., Sengupta, M., Cheng, R.K., Chia, J., Thirumalai, V., and Jesuthasan, S. (2017). Loss of the Habenula Intrinsic Neuromodulator Kisspeptin1 Affects Learning in Larval Zebrafish. eNeuro 4.
90. Mathuru, A.S., Kibat, C., Cheong, W.F., Shui, G.H., Wenk, M.R., Friedrich, R.W., and Jesuthasan, S. (2012). Chondroitin Fragments Are Odorants that Trigger Fear Behavior in Fish. Curr Biol 22, 538-544.
91. Kermen, F., Darnet, L., Wiest, C., Palumbo, F., Bechert, J., Uslu, O., and Yaksi, E. (2020). Stimulus-specific behavioral responses of zebrafish to a large range of odors exhibit individual variability. Bmc Biology 18.
92. Reiten, I., Uslu, F.E., Fore, S., Pelgrims, R., Ringers, C., Verdugo, C.D., Hoffman, M., Lal, P., Kawakami, K., Pekkan, K., et al. (2017). Motile-Cilia-Mediated Flow Improves Sensitivity and Temporal Resolution of Olfactory Computations. Curr Biol 27, 166-174.
93. Verdugo, C.D., Myren-Svelstad, S., Aydin, E., Van Hoeymissen, E., Deneubourg, C., Vanderhaeghe, S., Vancraeynest, J., Pelgrims, R., Cosacak, M.I., Muto, A., et al. (2019). Glia-neuron interactions underlie state transitions to generalized seizures. Nat Commun 10.
94. Viadimirov, N., Mu, Y., Kawashima, T., Bennett, D.V., Yang, C.T., Looger, L.L., Keller, P.J., Freeman, J., and Ahrens, M.B. (2014). Light-sheet functional imaging in fictively behaving zebrafish. Nat Methods 11, 883-884.
95. Valente, A., Huang, K.H., Portugues, R., and Engert, F.

(2012). Ontogeny of classical and operant learning behaviors in zebrafish. Learn Memory 19, 170-177.
96. Yashina, K., Tejero-Cantero, A., Herz, A., and Baier, H. (2019). Zebrafish Exploit Visual Cues and Geometric Relationships to Form a Spatial Memory. iScience 19, 119-134.
97. Dreosti, E., Lopes, G., Kampff, A.R., and Wilson, S.W. (2015). Development of social behavior in young zebrafish. Front Neural Circuit 9.
98. Hinz, R.C., and de Polavieja, G.G. (2017). Ontogeny of collective behavior reveals a simple attraction rule. P Natl Acad Sci USA 114, 2295-2300.
99. Golden, S.A., Heshmati, M., Flanigan, M., Christoffel, D.J., Guise, K., Pfau, M.L., Aleyasin, H., Menard, C., Zhang, H.X., Hodes, G.E., et al. (2016). Basal forebrain projections to the lateral habenula modulate aggression reward. Nature 534, 688-+.
100. Lecca, S., Meye, F.J., Trusel, M., Tchenio, A., Harris, J., Schwarz, M.K., Burdakov, D., Georges, F., and Mameli, M. (2017). Aversive stimuli drive hypothalamus-to-habenula excitation to promote escape behavior. Elife 6.
101. Mathis, V., and Lecourtier, L. (2017). Role of the lateral habenula in memory through online processing of information. Pharmacol Biochem Behav 162, 69-78.
102. Shabel, S.J., Proulx, C.D., Trias, A., Murphy, R.T., and Malinow, R. (2012). Input to the lateral habenula from the basal ganglia is excitatory, aversive, and suppressed by serotonin. Neuron 74, 475-481.
103. Sheth, C., Furlong, T.M., Keefe, K.A., and Taha, S.A. (2017). The lateral hypothalamus to lateral habenula projection, but not the ventral pallidum to lateral habenula projection, regulates voluntary ethanol consumption. Behav Brain Res 328, 195-208.
104. Diaz-Verdugo, C., Sun, G.J., Fawcett, C.H., Zhu, P.X., and Fishman, M.C. (2019). Mating Suppresses Alarm Response in Zebrafish. Curr Biol 29, 2541-+.
105. Kunst, M., Laurell, E., Mokayes, N., Kramer, A., Kubo, F., Fernandes, A.M., Forster, D., Dal Maschio, M., and Baier, H. (2019). A Cellular-Resolution Atlas of the Larval Zebrafish Brain. Neuron 103, 21-38 e25.
106. Lal, P., Tanabe, H., Suster, M.L., Ailani, D., Kotani, Y., Muto, A., Itoh, M., Iwasaki, M., Wada, H., Yaksi, E., et al. (2018). Identification of a neuronal population in the telencephalon essential for fear conditioning in zebrafish. BMC Biol 16, 45.
107. Marquart, G.D., Tabor, K.M., Horstick, E.J., Brown, M., Geoca, A.K., Polys, N.F., Nogare, D.D., and Burgess, H.A. (2017). High-precision registration between zebrafish brain atlases using symmetric diffeomorphic normalization. Gigascience 6.
108. Mueller, T., and Wullimann, M.F. (2009). An Evolutionary Interpretation of Teleostean Forebrain Anatomy. Brain Behav Evolut 74, 30-42.
109. Wullimann, M.F., and Rink, E. (2002). The teleostean forebrain: A comparative and developmental view based on early proliferation, Pax6 activity and catecholaminergic organization. Brain Res Bull 57, 363-370.
110. Rupprecht, P., and Friedrich, R.W. (2018). Precise Synaptic Balance in the Zebrafish Homolog of Olfactory Cortex. Neuron 100, 669-+.
111. Miyasaka, N., Arganda-Carreras, I., Wakisaka, N., Masuda, M., Sumbul, U., Seung, H.S., and Yoshihara, Y. (2014). Olfactory projectome in the zebrafish forebrain revealed by genetic single-neuron labelling. Nat Commun 5, 3639.
112. Yaksi, E., von Saint Paul, F., Niessing, J., Bundschuh, S.T., and Friedrich, R.W. (2009). Transformation of odor representations in target areas of the olfactory bulb. Nat Neurosci 12, 474-482.
113. Tabor, K.M., Marquart, G.D., Hurt, C., Smith, T.S., Geoca, A.K., Bhandiwad, A.A., Subedi, A., Sinclair, J.L., Rose, H.M., Polys, N.F., et al. (2019). Brain-wide cellular resolution imaging of Cre transgenic zebrafish lines for functional circuit-mapping. Elife 8.
114. Portavella, M., Duran, E., Gomez, Y., Torres, B., and Salas, C. (1998). Dorsomedial but not dorsolateral ablations disrupt avoidance response in a two-way active avoidance learning task in goldfish (Carassius auratus). Eur J Neurosci 10, 156-156.
115. Portavella, M., Vargas, J.P., Torres, B., and Salas, C. (2002). The effects of telencephalic pallial lesions on spatial, temporal, and emotional learning in goldfish. Brain Res Bull 57, 397-399.
116. Portavella, M., Torres, B., and Salas, C. (2004). Avoidance response in goldfish: Emotional and temporal involvement of medial and lateral telencephalic pallium. J Neurosci 24, 2335-2342.
117. Martin, I., Gomez, A., Salas, C., Puerto, A., and Rodriguez, F. (2011). Dorsomedial pallium lesions impair taste aversion learning in goldfish. Neurobiol Learn Mem 96, 297-305.
118. Elliott, S.B., and Maler, L. (2015). Stimulus-induced up states in the dorsal pallium of a weakly electric fish. J Neurophysiol 114, 2071-2076.
119. Ocana, F.M., Uceda, S., Arias, J.L., Salas, C., and Rodriguez, F. (2017). Dynamics of Goldfish Subregional Hippocampal Pallium Activity throughout Spatial Memory Formation. Brain Behav Evolut 90, 154-170.
120. Elliott, S.B., Harvey-Girard, E., Giassi, A.C.C., and Maler, L. (2017). Hippocampal-like circuitry in the pallium of an electric fish: Possible substrates for recursive pattern separation and completion. J Comp Neurol 525, 8-46.
121. Rodriguez-Exposito, B., Gomez, A., Martin-Monzon, I., Reiriz, M., Rodriguez, F., and Salas, C. (2017). Goldfish hippocampal pallium is essential to associate temporally discontiguous events. Neurobiol Learn Mem 139, 128-134.
122. Porter, B.A., and Mueller, T. (2020). The Zebrafish Amygdaloid Complex - Functional Ground Plan, Molecular Delineation, and Everted Topology. Front Neurosci-Switz 14.
123. Rodriguez, F., Lopez, J.C., Vargas, J.P., Gomez, Y., Broglio, C., and Salas, C. (2002). Conservation of spatial memory function in the pallial forebrain of reptiles and ray-finned fishes. J Neurosci 22, 2894-2903.
124. Wullimann, M.F., and Mueller, T. (2004). Teleostean and mammalian forebrains contrasted: Evidence from genes to behavior. J Comp Neurol 475, 143-162.
125. Aoki, T., Kinoshita, M., Aoki, R., Agetsuma, M., Aizawa, H., Yamazaki, M., Takahoko, M., Amo, R., Arata, A., Higashijima, S., et al. (2013). Imaging of neural ensemble for the retrieval of a learned behavioral program. Neuron 78, 881-894.

126. Fotowat, H., Lee, C., Jun, J.J., and Maler, L. (2019). Neural activity in a hippocampus-like region of the teleost pallium is associated with active sensing and navigation. Elife 8.
127. Mueller, T., Dong, Z.Q., Berberoglu, M.A., and Guo, S. (2011). The dorsal pallium in zebrafish, Danio rerio (Cyprinidae, Teleostei). Brain Res 1381, 95-105.
128. von Trotha, J.W., Vernier, P., and Bally-Cuif, L. (2014). Emotions and motivated behavior converge on an amygdala-like structure in the zebrafish. Eur J Neurosci 40, 3302-3315.
129. Wilczynski, W., and Northcutt, R.G. (1983). Connections of the Bullfrog Striatum - Efferent Projections. J Comp Neurol 214, 333-343.
130. Chen, W.Y., Peng, X.L., Deng, Q.S., Chen, M.J., Du, J.L., and Zhang, B.B. (2019). Role of Olfactorily Responsive Neurons in the Right Dorsal Habenula - Ventral Interpeduncular Nucleus Pathway in Food-Seeking Behaviors of Larval Zebrafish. Neuroscience.
131. Yaksi, E., Judkewitz, B., Friedrich, RW. (2007). Topological reorganization of odor representations in the olfactory bulb. PLoS Biol 5.
132. Kermen, F., Lal, P., Faturos, N.G., and Yaksi, E. (2020). Interhemispheric connections between olfactory bulbs improve odor detection. Plos Biology 18.
133. Suryanarayana, S.M., Perez-Fernandez, J., Robertson, B., and Grillner, S. (2021). Olfaction in Lamprey Pallium Revisited-Dual Projections of Mitral and Tufted Cells. Cell Rep 34, 108596.
134. Johnson, A.W., Crombag, H.S., Takamiya, K., Baraban, J.M., Holland, P.C., Huganir, R.L., and Reti, I.M. (2007). A selective role for neuronal activity regulated pentraxin in the processing of sensory-specific incentive value. J Neurosci 27, 13430-13435.
135. Wang, D.Q., Li, Y., Feng, Q.R., Guo, Q.C., Zhou, J.F., and Luo, M.M. (2017). Learning shapes the aversion and reward responses of lateral habenula neurons. Elife 6.
136. Mafra-Neto, A.C., R.T. (1994). Fine-scale structure of pheromone plumes modulates upwind orientation of flying moths Nature 369, 142–144.
137. Zimmer-Faust, R.K., Finelli, C.M., Pentcheff, N.D., and Wethey, D.S. (1995). Odor Plumes and Animal Navigation in Turbulent Water Flow: A Field Study. Biol Bull 188, 111-116.
138. Alvarez-Salvado, E., Licata, A.M., Connor, E.G., McHugh, M.K., King, B.M., Stavropoulos, N., Victor, J.D., Crimaldi, J.P., and Nagel, K.I. (2018). Elementary sensory-motor transformations underlying olfactory navigation in walking fruit-flies. Elife 7.
139. Vinepinsky, E., Cohen, L., Perchik, S., Ben-Shahar, O., Donchin, O., and Segev, R. (2020). Representation of edges, head direction, and swimming kinematics in the brain of freely-navigating fish. Sci Rep-Uk 10.
140. Aizawa, H., Yanagihara, S., Kobayashi, M., Niisato, K., Takekawa, T., Harukuni, R., McHugh, T.J., Fukai, T., Isomura, Y., and Okamoto, H. (2013). The Synchronous Activity of Lateral Habenular Neurons Is Essential for Regulating Hippocampal Theta Oscillation. J Neurosci 33, 8909-+.
141. Goutagny, R., Loureiro, M., Jackson, J., Chaumont, J., Williams, S., Isope, P., Kelche, C., Cassel, J.C., and Lecourtier, L. (2013). Interactions between the Lateral Habenula and the Hippocampus: Implication for Spatial Memory Processes. Neuropsychopharmacol 38, 2418-2426.
142. Baker, P.M., Rao, Y.X., Rivera, Z.M.G., Garcia, E.M., and Mizumori, S.J.Y. (2019). Selective Functional Interaction Between the Lateral Habenula and Hippocampus During Different Tests of Response Flexibility. Front Mol Neurosci 12.
143. Hildebrand, D.G.C., Cicconet, M., Torres, R.M.I., Choi, W., Quan, T.M., Moon, J., Wetzel, A.W., Champion, A.S., Graham, B.J., Randlett, O., et al. (2017). Whole-brain serial-section electron microscopy in larval zebrafish. Nature 545, 345-+.
144. Huang, K.H., Rupprecht, P., Frank, T., Kawakami, K., Bouwmeester, T., and Friedrich, R.W. (2020). A virtual reality system to analyze neural activity and behavior in adult zebrafish. Nat Methods 17, 343-+.
145. Wakisaka, N., Miyasaka, N., Koide, T., Masuda, M., Hiraki-Kajiyama, T., and Yoshihara, Y. (2017). An Adenosine Receptor for Olfaction in Fish. Curr Biol 27, 1437-+.
146. Furlan, G., Cuccioli, V., Vuillemin, N., Dirian, L., Muntasell, A.J., Coolen, M., Dray, N., Bedu, S., Houart, C., Beaurepaire, E., et al. (2017). Life-Long Neurogenic Activity of Individual Neural Stem Cells and Continuous Growth Establish an Outside-In Architecture in the Teleost Pallium. Curr Biol 27, 3288-+.
147. Lawson, R.P., Nord, C.L., Seymour, B., Thomas, D.L., Dayan, P., Pilling, S., and Roiser, J.P. (2017). Disrupted habenula function in major depression. Mol Psychiatry 22, 202-208.
148. Ranft, K., Dobrowolny, H., Krell, D., Bielau, H., Bogerts, B., and Bernstein, H.G. (2010). Evidence for structural abnormalities of the human habenular complex in affective disorders but not in schizophrenia. Psychol Med 40, 557-567.
149. Sartorius, A., Kiening, K.L., Kirsch, P., von Gall, C.C., Haberkorn, U., Unterberg, A.W., Henn, F.A., and Meyer-Lindenberg, A. (2010). Remission of major depression under deep brain stimulation of the lateral habenula in a therapy-refractory patient. Biol Psychiatry 67, e9-e11.
150. Morris, J.S., Smith, K.A., Cowen, P.J., Friston, K.J., and Dolan, R.J. (1999). Covariation of activity in habenula and dorsal raphe nuclei following tryptophan depletion. Neuroimage 10, 163-172.
151. Park, H.C., Kim, C.H., Bae, Y.K., Yeo, S.Y., Kim, S.H., Hong, S.K., Shin, J., Yoo, K.W., Hibi, M., Hirano, T., et al. (2000). Analysis of upstream elements in the HuC promoter leads to the establishment of transgenic zebrafish with fluorescent neurons. Dev Biol 227, 279-293.
152. Bergen, J.R., Anandan, P., Hanna, K.J., and Hingorani, R. (1992). Hierarchical Model-Based Motion Estimation. Lect Notes Comput Sc 588, 237-252.
153. Rupp, B., Wullimann, M.F., and Reichert, H. (1996). The zebrafish brain: A neuroanatomical comparison with the goldfish. Anat Embryol 194, 187-203.
154. Vladimirov, N., Mu, Y., Kawashima, T., Bennett, D.V., Yang, C.T., Looger, L.L., Keller, P.J., Freeman, J., and Ahrens, M.B. (2014). Light-sheet functional imaging in fictively behaving zebrafish. Nat Methods 11, 883-884.
155. Ahrens, M.B., Orger, M.B., Robson, D.N., Li, J.M., and Keller, P.J. (2013). Whole-brain functional imaging at cellular resolution using light-sheet microscopy. Nat Methods 10, 413-420.

MATERIALS AND METHODS

Fish husbandry:

NFSA (Norwegian Food Safety Authority) has approved the animal facility and fish maintenance. Fish were kept in 3,5L tanks in a Tecniplast ZebTec Multilinking System. Constant conditions were maintained: 28.5°C, pH 7.2, 700µSiemens. 14:10 hour light/dark cycle was preserved. Dry food (SDS100 up to 14dpf and SDS 400 for adult animals, Tecnilab BMI, the Netherlands) was given to fish twice a day, in addition to Artemia nauplii (Grade 0, Platinum Label, Argent Laboratories, Redmond, USA) once a day. From fertilization to 3dpf (days post fertilization) larvae were kept in a Petri dish with egg water (1.2g marine salt in 20L RO water, 1:1000 0.1% methylene blue) and between 3 and 5dpf in artificial fish water (AFW: 1.2 g marine salt in 20L RO water). Juvenile (3 to 4-week-old) zebrafish were used for the experiments.
For calcium imaging, Tg(elavl3:GCaMP5) (Jetti, Vendrell-Llopis, and Yaksi 2014) and Tg(elavl3:GCaMP6s) (Park et al. 2000) zebrafish lines were used.

Two-photon calcium imaging:

For in-vivo imaging, fish were embedded in 2-2,5% low-melting-point agarose (LMP, Fisher Scientific) in a recording chamber (Fluorodish, World Precision Instruments). To ensure odor to arrive to the nostrils, the LMP agarose was removed carefully in front of the nose, after solidifying for 20min. The constant perfusion of AFW bubbled with carbogen (95% O2 and 5%CO2) was maintained during the experiment.
For in-vitro imaging, brain explants were prepared as described in section "Dorsal dissection of juvenile zebrafish brain" below. The preparation is constantly perfused with artificial cerebrospinal fluid (ACSF) AFW was bubbled with carbogen (95% O2 and 5%CO2) throughout the experiment.
Two-photon microscopes were used for calcium imaging: Scientifica Inc, with a 16x water immersion objective; Nikon, NA 0.8, LWD 3.0 and Zeiss 7 MP with a 20x water immersion objective W Plan-Apochromat, NA 1.0. For excitation a mode-locked Ti:Sapphire laser (MaiTai Spectra-Physics) was tuned to 920nm. Recordings were performed as either single plane or volumetric recording (6-8 planes with a Piezo (Physik Instrumente (PI)). The acquisition rate was 6,4Hz for single plane recordings (image size 256x512 pixels) and between 2.3-3.4Hz per plane for volumetric scans (average image size 1536x750).

Odor preparation:

Our odor panel consisted of food odor, skin extract, urea, bile-acid mixture, amino acid mixture, and ammonium chloride. All odorants were purchased from Sigma Aldrich. Apart from food odor and skin extract, all odors were used at 10-4M concentration. Food odor was prepared using commercially available fish food; 1g of food particles was incubated in 50ml of fish water (FW) for at least 1 hour, filtered through filter paper, and diluted to 1:50. For skin extract (Kermen et al. 2020), adult zebrafish were first euthanized in ice-cold water and decapitated, the skin was peeled off from the body. 1g of skin was incubated in 2ml of AFW and was vortexed at 1300rpm for 1h at 4°C. After, the skin extract was dissolved in 50ml of AFW and filtered through the filter paper. All odors were prepared from the frozen stocks immediately before use.

Odor delivery:

The stimulation tube was positioned in front of the nose and the stimulus was delivered for 30s. The stimulation was performed with HPLC injection valve (Valco Instruments) controlled with Arduino Due. Before each experiment, a trial with fluorescein (10-4M in AFW) was performed to determine precise onset of odor delivery.

Micro-electrode stimulation:

Electrodes were pulled from a borosilicate glass microcapillary (1.00 mm; World Precision Instruments) using a laser puller (Sutter Instruments co. Model P-2000). Electrodes tips were were broken so that the final tip diameter of the stimulating electrode was around 10-15µm. The electrode was filled with artificial cerebro-spinal fluid (ACSF). Two-separate electrodes were connected to two poles of the ISO-flex stimulus isolator (A.M.P.I.), and electrodes were glued by two-component epoxy so that the electrode tips are close to each other (within 1-2 mm). Only a single electrode tip was inserted and positioned in the brain explant using a micromanipulator (Scientifica, UK), and the other tip was left outside the brain. A train of short current pulses (2-5µA) for 50 milliseconds duration and 20 seconds inter stimulus intervals was applied to the target brain region, using a computer-controlled Arduino Due as a stimulus generator.

Dissection of juvenile zebrafish brain explant:

All animals (3-4 weeks post fertilization) were anesthetized in ice-cold artificial fish water (AFW) and euthanized by decapitation in oxygenated artificial cerebro-spinal fluid (ACSF). The dissection was carried out in ACSF. After removing jaws and eyes, muscle tissue, gills and fat were cleaned to allow oxygen diffusions

to the brain explant. Next, the skin tissue, bone and dura mater covering the forebrain was removed from the dorsal side, allowing electrode access.

Data analysis:

Two-photon microscopy images were aligned using a method described in (Reiten et al. 2017; Verdugo et al. 2019). Occasional XY drift was corrected, based on "hierarchical model-based motion estimation" (Bergen et al. 1992). Recordings were then visually inspected for remaining motion and Z-drift, recordings with remaining motion artifacts were discarded. Regions of interest (ROIs) corresponding to neurons were automatically detected using a template matching algorithm (Jetti, Vendrell-Llopis, and Yaksi 2014; Verdugo et al. 2019), and visually confirmed. To calculate the time course of each neuron, pixels belonging to each ROI were averaged over time. For each ROI, fractional change in fluorescence ($\Delta F/F$) relative to baseline was calculated.

Neurons were clustered into functional clusters using k-means clustering algorithm in MATLAB (Figure 1A, Figure 2B, Figure 3E) (Jetti, Vendrell-Llopis, and Yaksi 2014). For Figure 2 an average activity of all neurons in each cluster of the habenula was averaged. This population vector was used as a reference activity and correlated with each neuron in the telencephalon.

Delineation of brain regions in the telencephalon was done manually on the raw image of the brain (as in Figure 2E) based on anatomical landmarks (Rupp, Wullimann, and Reichert 1996) described in previous studies in zebrafish and other teleost fish (Diaz-Verdugo et al. 2019; Huang et al. 2020; Wullimann and Mueller 2004; Elliott et al. 2017; Fotowat et al. 2019; Rodriguez-Exposito et al. 2017).

Cluster selectivity was calculated to quantify the overlap of manually delineated brain regions with functional clusters of neurons identified using k-means clustering based on their spontaneous activity. Cluster selectivity index is the life-time sparseness (Jetti, Vendrell-Llopis, and Yaksi 2014) for the distribution of neurons within an anatomically defined brain region across the k-means clusters. If cluster selectivity is 1, it means that neurons of an anatomically identified brain region belong to one functional cluster. If cluster selectivity is 0, all neurons of an anatomically identified brain region are equally distributed into all functional k-means clusters.

Cluster fidelity was calculated by measuring the probability of pairs of neurons being in the same cluster during two different time periods (Jetti, Vendrell-Llopis, and Yaksi 2014). We compared the cluster fidelity of real k-means clusters with shuffled the cluster identities of same neurons.

In Figure 4, neurons were stimulated 6 times with each stimulus: odor, micro-stimulation and odor + micro-stimulation. Neurons were considered as responsive if their response (5s) exceeded 2 standard deviations above the 5s-baseline period preceding the stimulation. To calculate how odor and micro-stimulation influenced each other, we compared whether these two different stimuli can significantly (using Wilcoxon signed rank test) change each other when delivered simultaneously (odor + micro-stimulation).

For Figure 5, odor responses of habenular neurons were classified by correlating their odor response with a step function, as previously described in (Cheng et al. 2017). Top 5% of habenular neurons with highest or lowest correlations were considered as strongly excited or inhibited, respectively. Averaged ongoing activity preceding the stimulation in those classified habenular neurons was used as a reference vector and correlated with each forebrain neuron to identify forebrain neurons that are highly correlated with excited or inhibited habenular neurons.

Statistics:

Statistical analysis was done using MATLAB; p-values are represented in the figure legends as (*$p<0.05$, **$p<0.01$, ***$p<0.001$). Wilcoxon ranksum test was used for non-paired comparisons and Wilcoxon signed rank test for paired comparisons.

All analysis was performed with Fiji and MATLAB.